System Identification for Small, Low-Cost, Fixed-Wing Unmanned Aircraft

Andrei Dorobantu*, Austin Murch†, Bérénice Mettler‡, and Gary Balas§

Department of Aerospace Engineering & Mechanics

University of Minnesota, Minneapolis, MN, 55455, USA

This paper describes a practical system identification procedure for small, low-cost, fixed-wing unmanned aircraft. Physical size and cost restrictions limit the sensing capabilities of these vehicles. The procedure is demonstrated on an Ultra Stick 25e, therefore emphasizing a minimum complexity approach compatible with a low-cost inertial sensor. A linear model, obtained from the generic nonlinear equations of motion for aircraft, is used as a basis for system identification. This model is populated with results from a first principles analysis to form a baseline model. Flight experiments are designed using the baseline model and operational constraints to collect informative data. Parameters of the linear model are identified by fitting the model to frequency responses extracted from the data. The parameters are integrated into the nonlinear equations of motion, and both linear and nonlinear models are validated in the time domain. Verification of model accuracy is extended with a sensitivity and residual analysis.

*PhD Candidate, Department of Aerospace Engineering & Mechanics, 107 Akerman Hall, 110 Union St. SE, Minneapolis, MN 55455, AIAA Student Member, dorob002@aem.umn.edu

†Senior Research Associate, Department of Aerospace Engineering & Mechanics, 107 Akerman Hall, 110 Union St. SE, Minneapolis, MN 55455, AIAA Senior Member, murch@aem.umn.edu

‡Assistant Professor, Department of Aerospace Engineering & Mechanics, 107 Akerman Hall, 110 Union St. SE, Minneapolis, MN 55455, AIAA Member, mettler@aem.umn.edu

§Professor, Department of Aerospace Engineering & Mechanics, 107 Akerman Hall, 110 Union St. SE, Minneapolis, MN 55455, AIAA Associate Fellow, balas@aem.umn.edu

Nomenclature

m	Mass, kg
I	Moment of inertia, $kg\ m^2$
g	Gravity, m/s^2
ϕ, θ, ψ	Attitude angles, rad
u, v, w	Body-axis velocities, m/s
p, q, r	Body-axis angular rates, rad/s
a_x, a_y, a_z	Body-axis measured accelerations, m/s^2
δ_{elev}	Elevator deflection, rad
δ_{ail}	Aileron deflection, rad
δ_{rud}	Rudder deflection, rad
X, Y, Z	Aerodynamic forces, N
L, M, N	Aerodynamic moments, $N\ m$
T	Thrust force, N
S	Spectral density function
γ^2	Coherence function

I. Introduction

Unmanned aerial vehicles (UAVs) have become popular as fight test platforms in control research applications. An important task for the development of these platforms is modeling the aircraft dynamics. System identification techniques, which rely on experimental data obtained in flight, have been developed to accomplish this task efficiently. However, the application of system identification techniques to small, low-cost UAVs poses a challenge. Physical airframe size and cost restrictions limit the availability and quality of onboard sensors. For example, sensors required to measure angle-of-attack or angle-of-sideslip may not be available. Furthermore, the available sensors may be susceptible to high levels of noise. This challenge is addressed with a practical procedure to identify the dynamics of small, fixed-wing UAVs using a commercial low-cost inertial sensor.

Foundations and mathematical background of system identification theory are covered in detail by References 1 and 2. References 3, 4, and 5 summarize various engineering approaches to system identification, including time domain and frequency domain methods. Novel identification techniques have been published in recent literature, detailing advancements in areas such as real-time identification and efficient control surface input design.[6–12] Computational software tools are also readily available to automate parts of the system

identification process.[1,3,4] What remains unclear, however, is the viability of the various techniques for application to small, low-cost UAVs. For example, some techniques assume that highly accurate sensor measurements are available, while others require measurement of the full aerodynamic state. These assumptions are unrealistic for low-cost platforms.

The procedure described in this paper is based on system identification in the frequency domain. A linear state-space model is derived from the generic nonlinear equations of motion for aircraft. Parameters in the linear model are identified by fitting the model to frequency responses extracted from flight data, based on the approach in Reference 3. This approach is similar to the frequency domain output-error methods in References 4 and 12, but relies on a different cost function. It also implements a different algorithm to transform flight data into the frequency domain. Both methods share the advantage of fitting models over frequency ranges relevant to aircraft dynamics, and neither requires measurement of every state in the model. Using frequency responses, however, preserves insightful ties to flight dynamics and Bode plots. Its drawbacks include the need for longer and less efficient flight experiments.[12] The procedure is applied to an Ultra Stick 25e UAV operated by the University of Minnesota,[13] shown in Figure 1. Similar analysis has been applied to small, low-cost, rotorcraft UAVs.[6–8] This paper broadens the preliminary fixed-wing results given in Reference 14.

Figure 1. University of Minnesota Ultra Stick 25e UAV.

Remaining sections of the paper are organized as follows: Section II provides the nonlinear equations of motion, linearized model, and simplifying assumptions. Physical properties of the UAV and the first principles analysis used to obtain a baseline model are described in Section III. Flight experiments used to collect informative data are designed using the baseline model and operational constraints in Section IV. Section V briefly describes the theory behind frequency domain system identification, and results are given in Section VI. The identified parameters are integrated into the nonlinear equations of motion, and Section VII shows time domain validation results for both linear and nonlinear models. Section VIII describes a sensitivity and residual analysis, and Section IX gives concluding remarks.

II. Fixed-Wing Aircraft Dynamics

A nonlinear model for fixed-wing aircraft dynamics can be derived from the generic rigid-body equations of motion. Conventional aircraft are subject to external forces and moments due to gravity, propulsion, and aerodynamics. The central modeling task is to determine expressions for these external forces and moments. A simple nonlinear model is obtained when the equations of motion are written in the vehicle body-axis (see References 4 and 15). Standard nomenclature is used for the states: x-y-z body-axis velocities (u, v, w), x-y-z body-axis angular rates (p, q, r), and a standard 3-2-1 ordered rotation sequence of Euler angles (ϕ, θ, ψ). The x-y-z body-axis aerodynamic forces are denoted X, Y, and Z, and the x-y-z body-axis aerodynamic moments are denoted L, M, and N.

For simplicity, gyroscopic effects of the rotating mass of the motor are assumed to be insignificant, and the thrust T is assumed to act through the center of gravity and coincide with the body x-axis. The resulting system is summarized by the following equations:[4]

Force Equations:

$$\dot{u} = (rv - qw) + X/m - g\sin\theta + T/m \tag{1}$$

$$\dot{v} = (pw - ru) + Y/m + g\cos\theta\sin\phi \tag{2}$$

$$\dot{w} = (qu - pv) + Z/m + g\cos\theta\cos\phi \tag{3}$$

Moment Equations:

$$\dot{p} - (I_{xz}/I_x)\dot{r} = -qr(I_z - I_y)/I_x + qpI_{xz}/I_x + L/I_x \tag{4}$$

$$\dot{q} = -pr(I_x - I_z)/I_y - (p^2 - r^2)I_{xz}/I_y + M/I_y \tag{5}$$

$$\dot{r} - (I_{xz}/I_z)\dot{p} = -pq(I_y - I_x)/I_z - qrI_{xz}/I_z + N/I_z \tag{6}$$

Kinematic Equations:

$$\dot{\phi} = p + \tan\theta(q\sin\phi + r\cos\phi) \tag{7}$$

$$\dot{\theta} = q\cos\phi - r\sin\phi \tag{8}$$

$$\dot{\psi} = \sec\theta(q\sin\phi + r\cos\phi) \tag{9}$$

The dynamic response of an aircraft can be recorded with an Inertial Measurement Unit (IMU). Low-cost sensors measure angular rates (p, q, r) and translational accelerations (a_x, a_y, a_z).[16] The measured accelerations, however, exclude the effect of gravity:[4]

$$a_x = \dot{u} - (rv - qw) + g\sin\theta \tag{10}$$

$$a_y = \dot{v} - (pw - ru) - g\cos\theta\sin\phi \tag{11}$$

$$a_z = \dot{w} - (qu - pv) - g\cos\theta\cos\phi \tag{12}$$

The nonlinear model is linearized by assuming small perturbations from a steady, level trim condition. For simplicity, state variables in the nonlinear equations of motion are recast using the same notation as perturbation states in the linear model. The longitudinal dynamics are decoupled from the lateral/directional dynamics, and the thrust is assumed to be constant.

1. *Longitudinal Dynamics*

The longitudinal dynamics are described by the states $x_{lon} = [u, w, q, \theta]^\top$, which correspond to Equations 1, 3, 5, and 8. The forces X and Z, and the moment M are assumed to be linear functions of u, w, q, and the elevator deflection δ_{elev}, resulting in the following system:

$$\dot{x}_{lon} = A_{lon} x_{lon} + B_{lon} \delta_{elev} \tag{13}$$

where

$$A_{lon} = \begin{bmatrix} X_u & X_w & X_q - W_e & -g\cos\theta_e \\ Z_u & Z_w & Z_q + U_e & -g\sin\theta_e \\ M_u & M_w & M_q & 0 \\ 0 & 0 & 1 & 0 \end{bmatrix} \quad B_{lon} = \begin{bmatrix} X_{\delta_{elev}} \\ Z_{\delta_{elev}} \\ M_{\delta_{elev}} \\ 0 \end{bmatrix}$$

The terms W_e, U_e, and θ_e represent the trim condition. The X, Z, and M terms with subscripts are the dimensional aerodynamic derivatives to be identified. Coefficients in the A_{lon} matrix are the stability derivatives, and the B_{lon} matrix holds the control derivatives. Finally, the linearized acceleration measurements are given by:

$$a_x = \dot{u} + qW_e + g\cos\theta_e\,\theta + g\sin\theta_e \tag{14}$$

$$a_z = \dot{w} - qU_e + g\sin\theta_e\,\theta - g\cos\theta_e \tag{15}$$

The longitudinal dynamics can be decoupled further into the phugoid and the short-period modes. The phugoid mode is typically very slow, lightly damped, and dominates the response in u, θ, and a_x. The short-period mode is typically fast, moderately damped, and dominates the response in w, q, and a_z. For control applications, accurate knowledge of the phugoid mode is not crucial due to the low frequency of the oscillation, which is compensated for with feedback control. Stability and performance characteristics also depend primarily on the short-period mode.[15] System identification is applied to the short-period model shown in the following system, where the state vector is $x_{lon} = [w, q]^\top$:

$$A_{lon} = \begin{bmatrix} Z_w & Z_q + U_e \\ M_w & M_q \end{bmatrix} \quad B_{lon} = \begin{bmatrix} Z_{\delta_{elev}} \\ M_{\delta_{elev}} \end{bmatrix} \tag{16}$$

Terms in Equations 14 and 15 that depend on θ are neglected for the short-period model. Furthermore, the short-period aircraft response captured by a_x is small relative to the measurement noise on a low-cost IMU. Hence, a_x is not used in this identification analysis.

2. Lateral/Directional Dynamics

The lateral/directional dynamics are described by the states $x_{lat} = [v, p, r, \phi, \psi]^\top$, which correspond to Equations 2, 4, 6, 7, and 9. Force Y, and moments L and N are described by linear functions of v, p, r, and aileron and rudder deflections (δ_{ail} and δ_{rud}, respectively). The resulting system is given by the following:

$$M_{lat}\dot{x}_{lat} = A'_{lat}x_{lat} + B'_{lat}\begin{bmatrix}\delta_{ail}\\ \delta_{rud}\end{bmatrix} \tag{17}$$

where

$$M_{lat} = \begin{bmatrix} 1 & 0 & 0 & 0 & 0 \\ 0 & 1 & -I_{xz}/I_x & 0 & 0 \\ 0 & -I_{xz}/I_z & 1 & 0 & 0 \\ 0 & 0 & 0 & 1 & 0 \\ 0 & 0 & 0 & 0 & 1 \end{bmatrix}$$

$$A'_{lat} = \begin{bmatrix} Y_v & Y_p + W_e & Y_r - U_e & g\cos\theta_e & 0 \\ L_v & L_p & L_r & 0 & 0 \\ N_v & N_p & N_r & 0 & 0 \\ 0 & 1 & \tan\theta_e & 0 & 0 \\ 0 & 0 & \sec\theta_e & 0 & 0 \end{bmatrix} \quad B'_{lat} = \begin{bmatrix} Y_{\delta_{ail}} & Y_{\delta_{rud}} \\ L_{\delta_{ail}} & L_{\delta_{rud}} \\ N_{\delta_{ail}} & N_{\delta_{rud}} \\ 0 & 0 \\ 0 & 0 \end{bmatrix}$$

The Y, L, and N terms with subscripts in A'_{lat} and B'_{lat} are the dimensional aerodynamic derivatives to be identified. Unlike the longitudinal dynamics, the lateral/directional dynamics cannot be decoupled into independent modes. They are governed by a slow spiral mode, a fast lightly damped dutch roll mode, and an even faster roll mode. Finally, the linearized acceleration measurement is given by:

$$a_y = \dot{v} - pW_e + rU_e - g\cos\theta_e\,\phi \tag{18}$$

The longitudinal and lateral/directional systems form a linear parametric model that is used as a basis for frequency domain system identification. Stability and control derivatives are identified by fitting these models to frequency responses extracted from flight data.

III. UAV Airframe and Preliminary Analysis

This section presents the physical properties of the Ultra Stick 25e vehicle, its hardware and sensing capabilities, and the preliminary analysis used to generate a baseline model of the aircraft dynamics. The baseline model is analyzed to determine the approximate gain and bandwidth of the system. This a priori insight is used to design informative and efficient flight experiments for the subsequent frequency domain system identification.

A. Airframe and Instrumentation

The Ultra Stick 25e has a conventional fixed-wing airframe with aileron, rudder, and elevator control surfaces. The aircraft is also equipped with flaps, but these are not used in this analysis. All control surfaces are actuated via electric servos with a maximum deflection of 25 degrees in each direction. The propulsion system consists of an electric motor that drives a fixed-pitch propeller. Physical properties of the airframe are summarized in Table 1, where the moments of inertia are calculated using swing tests. More details on the University of Minnesota Ultra Stick 25e platform can be found in References 13 and 17.

Table 1. Physical properties of the Ultra Stick 25e airframe.

Property	Symbol	Value	Units
Mass	m	1.959	kg
Wing Span	b	1.27	m
Wing Area	S	0.31	m^2
Mean Aerodynamic Chord	c	0.25	m
Moment of Inertia	I_x	0.089	$kg\ m^2$
Moment of Inertia	I_y	0.144	$kg\ m^2$
Moment of Inertia	I_z	0.162	$kg\ m^2$
Cross Moment of Inertia	I_{xz}	0.014	$kg\ m^2$

The aircraft is instrumented with an IMU that provides measurements of angular rates and translational accelerations.[16] Three gyroscopes form the angular rate sensor, and three accelerometers form the acceleration sensor. A ground test, with the throttle set to around 70%, resulted in a noise amplitude is approximately 2 deg/s in each angular rate channel, and 0.5 m/s^2 in each acceleration channel. The aircraft is also equipped with an on-board flight computer.[18] Manual pilot commands are recorded by the flight computer prior to being delivered to the actuators. This is useful for system identification flight experiments, where augmenting manual pilot commands with automatically generated excitation signals helps maintain the aircraft near the trim condition. The flight computer delivers actuator commands at 50 Hz, and the IMU data is recorded at the same rate.

Flight tests are limited to line-of-sight range to avoid communication dropout, for safety, and to satisfy FAA regulations for radio controlled aircraft. The pilot on the ground must always be able to re-gain manual control of the aircraft, and performs all take-offs and landings. The aircraft systems are battery powered, allowing 20 minutes of flying time on a single charge.

B. Preliminary Analysis

The task of system identification can be greatly simplified by incorporating a priori knowledge of the aircraft dynamics into the analysis. A baseline model is generated to gain insight into the general characteristics of the system, such as its gain and bandwidth. This information is used as a guide to design informative and efficient system identification flight experiments, for which a rough approximation of the dynamics is sufficient.

Various methods can be applied to obtain a baseline model. If the airframe is similar to an already modeled aircraft, its model can be scaled. However, if the aircraft configuration and airfoils are new, empirical methods and/or simple wind tunnel tests can be implemented. For example, the Digital DATCOM[19] is a purely empirical guide to estimating stability and control derivatives based on aircraft configuration and the experience of engineers. Simple wind tunnel tests can also be used, in particular to obtain estimates of control derivatives and stability derivatives associated with the body velocity components u, v, and w. The key point is that various methods exist to obtain a baseline model, and depending on the available resources, a combination of methods can be used.

A baseline model of the Ultra Stick 25e flight dynamics is generated using aerodynamic data from two similar airframes. Control derivatives and stability derivatives associated with the body velocities are estimated from wind tunnel tests performed with an Ultra Stick Mini. This airframe is smaller than the 25e and fits in the wind tunnel available at the University of Minnesota. The 25e and the Mini have similar aerodynamics but are not exact geometric scales of each other. Stability derivatives associated with the angular rates are taken from an aerodynamic model for the Ultra Stick 120.[13] This airframe is larger than the 25e, has similar aerodynamics, yet it also is not an exact geometric scale. The aerodynamic model for the 120 was developed at NASA Langley Research Center, using both static and dynamic wind tunnel testing.[20,21] Due to these approximations in the aerodynamics, the baseline model for the Ultra Stick 25e is only used as a guide to design flight experiments.

For the wind tunnel tests performed on the Ultra Stick Mini, airspeed is held constant while aerodynamic forces and moments on the aircraft are measured by a sensor. The first two tests consist of static variations in angle-of-attack and angle-of-sideslip. These tests are sufficient to obtain estimates of the stability derivatives associated with the body velocity components. A third wind tunnel test is conducted to estimate the control derivatives.

In this test, each control surface is deflected independently while aerodynamic forces and moments are measured.

1. *Longitudinal Dynamics*

The longitudinal control derivatives, velocity stability derivatives, and equilibrium terms are estimated using wind tunnel data acquired with the Ultra Stick Mini. The angular rate stability derivatives are taken from values estimated for the Ultra Stick 120.[20,21] Along with mass data from Table 1, the longitudinal baseline model is constructed and given by:

$$A_{lon} = \begin{bmatrix} -0.38 & 0.60 & -0.36 & -9.80 \\ -0.98 & -7.81 & 15.32 & -0.21 \\ 0.18 & -8.31 & -35.21 & 0 \\ 0 & 0 & 1 & 0 \end{bmatrix} \quad B_{lon} = \begin{bmatrix} -0.36 \\ -3.62 \\ -106.32 \\ 0 \end{bmatrix}$$

The modes of the longitudinal dynamics are computed from an eigenvalue decomposition of the system state matrix and presented in Table 2.

Table 2. Estimated modes of the longitudinal dynamics.

Mode	Natural Frequency [rad/s]	Damping Ratio
Phugoid	0.48	0.43
Short-Period Pole 1	13.70	-
Short-Period Pole 2	29.28	-

The phugoid mode has a natural frequency of 0.48 rad/s with a damping ratio of 0.43. The typical short-period mode does not appear in the baseline model. Instead, it is replaced by two stable real poles at 13.70 and 29.28 rad/s. This is unconventional for fixed-wing aircraft and is a result of estimating derivatives using the Ultra Stick Mini and 120. However, this result is not a major concern for the baseline model since the approximate bandwidth associated with the longitudinal dynamics can still be inferred.

2. *Lateral/Directional Dynamics*

The lateral/directional control derivatives, velocity stability derivatives, and equilibrium terms are estimated using wind tunnel data acquired with the Ultra Stick Mini. The angular rate stability derivatives are taken from values estimated for the Ultra Stick 120.[20,21] The

populated matrices are shown by the following:

$$M_{lat} = \begin{bmatrix} 1 & 0 & 0 & 0 & 0 \\ 0 & 1 & -0.157 & 0 & 0 \\ 0 & -0.086 & 1 & 0 & 0 \\ 0 & 0 & 0 & 1 & 0 \\ 0 & 0 & 0 & 0 & 1 \end{bmatrix}$$

$$A'_{lat} = \begin{bmatrix} -1.64 & 0.64 & -18.90 & 9.50 & 0 \\ -2.14 & -13.71 & 13.71 & 0 & 0 \\ 0.93 & -0.12 & -7.28 & 0 & 0 \\ 0 & 1 & 0.03 & 0 & 0 \\ 0 & 0 & 1 & 0 & 0 \end{bmatrix} \quad B'_{lat} = \begin{bmatrix} 0 & 6.99 \\ -68.65 & 18.32 \\ -8.03 & -19.01 \\ 0 & 0 \\ 0 & 0 \end{bmatrix} \tag{19}$$

The modes of the lateral/directional dynamics are computed from an eigenvalue decomposition of the system state matrix, and are presented in Table 3.

Table 3. Estimated modes of the lateral/directional dynamics.

Mode	Natural Frequency [rad/s]	Damping Ratio
Spiral	0.05	-
Dutch Roll	6.03	0.77
Roll	12.38	-

The spiral mode is represented by a pole at 0.05 rad/s, the dutch roll mode has natural frequency of 6.03 rad/s with damping ratio 0.77, and the roll mode is represented by a pole at 12.38 rad/s.

IV. Design of Flight Experiments

Typical flight experiments for small UAVs platforms under development are divided into three segments: take-off, research experiments, and landing. Each flight begins with a manual take-off by the pilot. Once airborne, the pilot flies the aircraft into a race track pattern with constant altitude and obtains a steady, level trim. The race track pattern is used to maximize the available straight and level flight time. Dimensions of the pattern are defined by line of sight requirements. In an emergency, the pilot must always be able to re-gain manual control of the aircraft and visually guide it back to safe operation. As a result of these constraints, the Ultra Stick 25e can only achieve a 20 second maximum time window of straight and level flight.

Research experiments begin when the pilot is ready to engage the on-board flight computer. Immediately following a turn in the race track pattern, the pilot trims the aircraft to a desired flight condition. In this case, the flight condition for the Ultra Stick 25e is straight and level flight at approximately 19 m/s. The pilot then engages the flight computer to execute the research experiment. When the experiment is complete, the pilot disengages the flight computer and continues the race track pattern. The pilot can choose to realign the aircraft for additional experiments, or to conclude the flight test with a manual landing.

A. System Identification Experiments

The aircraft dynamics must be excited during a flight experiment in order to successfully perform system identification. Automatic frequency sweep inputs are used to accomplish this over a broad frequency range. These inputs are computer generated sinusoids with frequencies that vary logarithmically with time. The flight computer applies signals for one control surface at a time in order to prevent correlation between the inputs. Frequency sweeps are designed using the default logarithmic chirp function in MATLAB,[22] which implements the following equation:

$$\delta(t) = A \sin\big(f(t)t\big), \qquad \text{where} \qquad f(t) = f_0 \left(\frac{f_1}{f_0}\right)^{t/t_1} \tag{20}$$

In this relationship, the amplitude A is specified, as well as a frequency interval given by f_0 and f_1 (in Hz). A time vector t is required, where the final time is given by t_1.

Frequency sweep inputs can take the aircraft away from the trim condition.[3,4] To counter this effect, the inputs are augmented with a manual pilot input via the flight computer. The pilot counters the drift by ensuring that the nose and wings remain level over the course of the maneuver. Pilot augmentation is only permitted for the control surface on which the active frequency sweep is applied. All remaining control surfaces are fixed at their trim values throughout the experiment. If multiple inputs were active simultaneously, the extracted frequency response would need to be conditioned for the effect of the secondary input on the primary input-output response. To ensure that each experiment begins with airspeed close to 19 m/s, the throttle setting is fixed to 70%. Besides frequency sweep experiments, flight data from doublet maneuvers is collected to validate the identified dynamics in the time domain. To obtain this data, the pilot executes a manual doublet for each control surface.

Several practical factors constrain the design of frequency sweeps experiments. Due to trimming requirements before and after each turn, a 10 second experiment time window is the approximate limit for the Ultra Stick 25e. As a result, dynamics at frequencies below 0.1 Hz cannot be identified accurately. Given a data sampling rate of 50 Hz, the Nyquist limit indicates that signals above 25 Hz cannot be recorded accurately. A more practical

limit for system identification is closer to 10 Hz.[3] The fastest pole in the baseline model is located around 30 rad/s, or about 5 Hz. Hence, the upper frequency limit is not a major concern. The phugoid and spiral modes are located below 0.1 Hz. They cannot be identified accurately due to a lack of excitation in this frequency range. However, this is not of great concern as the slow nature of these dynamics can be easily handled by a pilot or a control system.

Servo actuator dynamics must also be considered in the design of system identification experiments. Specifications on actuator bandwidth are often unavailable from low-cost hobby manufacturers. Ground tests on the Ultra Stick 25e indicated that the bandwidth of the servos is below 15 Hz. Therefore, frequency sweeps from 0.1 to 15 Hz would adequately excite the flight dynamics relevant for control applications as well as the actuator dynamics.

B. Frequency Sweep Design

Figure 2 shows the baseline model frequency response for each control surface to its corresponding primary angular rate response. Conventional aircraft dynamics are dominated by these input-output relationships. Accurate models for these relationships are thus a key requirement for control applications. The 0.1 to 15 Hz frequency range is highlighted by the solid curves.

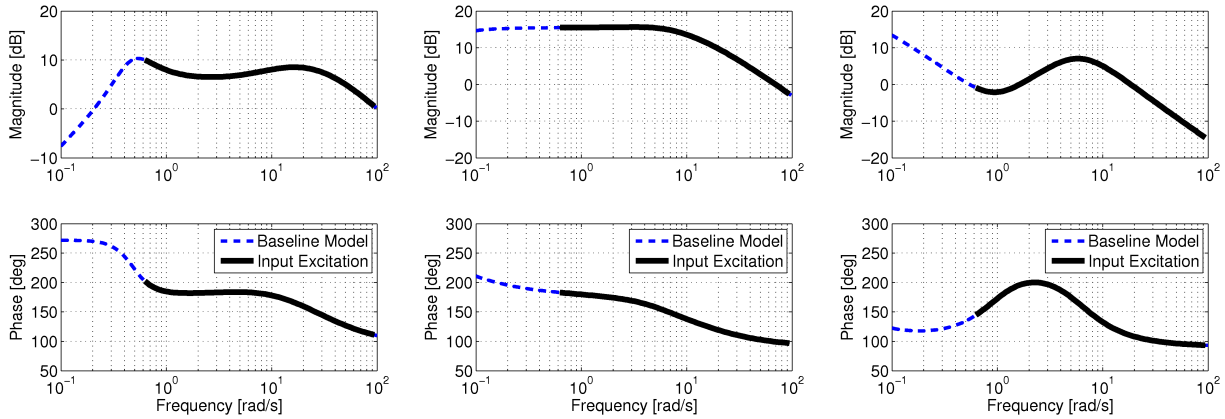

(a) Elevator to pitch rate. (b) Aileron to roll rate. (c) Rudder to yaw rate.

Figure 2. Baseline model frequency response with range for system identification.

To achieve a sufficiently high signal-to-noise ratio (SNR) on the Ultra Stick 25e, the measured output response must exceed 6 deg/s for the angular rates, and 1.5 m/s^2 for the accelerations. This accounts for about a factor of 3 between the magnitude of the noise and the magnitude of the response, which represents the minimum desired SNR.[3] Experience has shown that higher SNR, closer to a value of 6, can improve the quality of the frequency responses. A frequency sweep with amplitude of 4 degrees is chosen for safety and to satisfy

SNR requirements. Higher amplitudes would generally be considered unsafe due to the uncertainty in the baseline model.

The identification frequency range is broken down into two intervals: low and high frequency. Each interval has a dedicated experiment to ensure that the entire frequency range is excited sufficiently. The low frequency interval spans 0.1 to 5 Hz, and the high frequency interval spans 4 to 15 Hz. Five frequency sweep experiments are conducted for each interval on each control surface to obtain a rich data set. Multiple runs are required because frequency responses are ultimately extracted from the flight data using an averaging process. Figure 3 shows both simulation and flight results from a low frequency aileron sweep. The pilot command augmentation is clearly visible on the right.

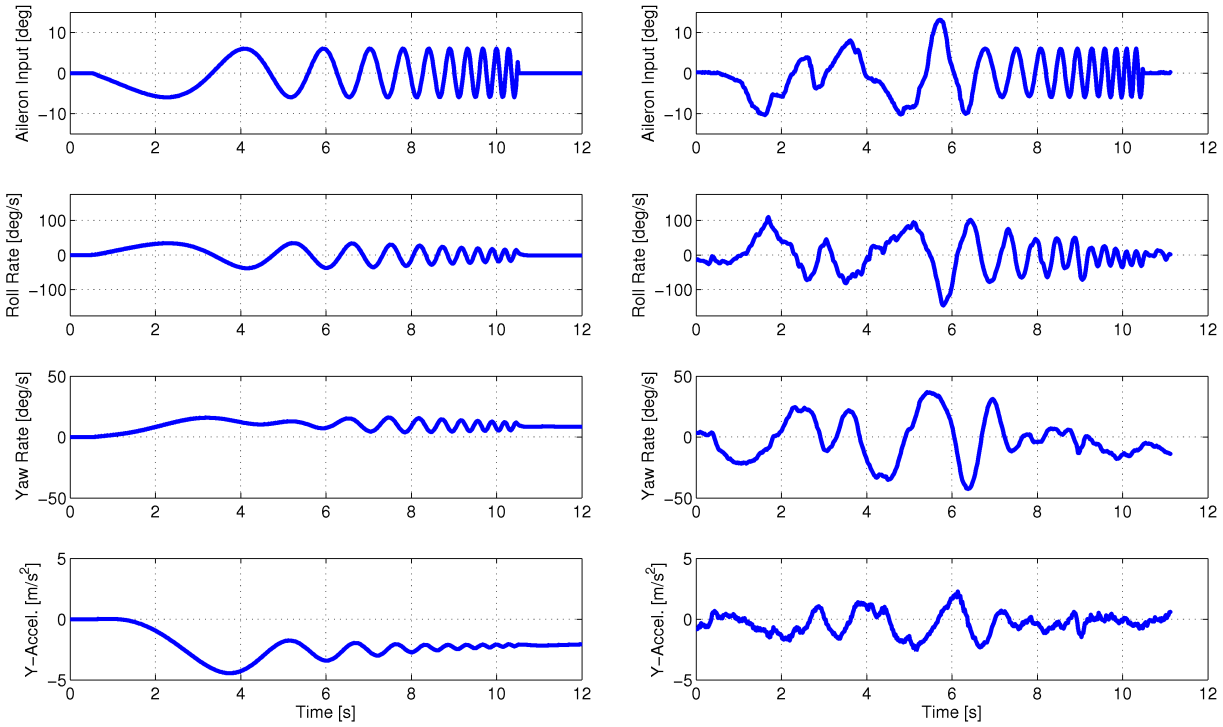

(a) Aileron sweep baseline model simulation.

(b) Aileron sweep flight experiment data.

Figure 3. Sample aileron frequency sweep input signal and response.

The flight data in Figure 3 shows that the manual pilot augmentation helps keep the aircraft around the desired trim condition during the frequency sweep experiment. The pilot is able to maintain oscillations about the trim condition without canceling out the input excitation, eliminating the bias noted at the end of the maneuver in the baseline simulation. The true aircraft exhibits higher gain in the roll rate channel than predicted by the baseline model. However, the baseline model accurately predicts low gain in the off-axis, particularly in the y-component acceleration response.

V. Frequency Domain System Identification

The frequency domain system identification process is comprised of two steps. The first identification step extracts frequency responses using spectral quantities computed from the input-output flight data. In this paper, control surface commands recorded by the flight computer are considered inputs because sensors are not available to measure the true surface deflections. The second identification step fits the linear state-space models (described by Equations 16 and 17) to the extracted frequency responses. Parameters in the linear models are identified through a nonlinear optimization that minimizes the fitting error in the frequency domain.

A. Extracting Frequency Responses

The basic frequency domain identification problem is cast for a two-input, single-output system without the loss of generality.[23] This formulation can easily be modified to include additional inputs. A multiple-output model, such as the lateral/directional aircraft model, is constructed by superposing sets of multiple-input, single-output relationships. The block diagram in Figure 4 shows the fundamental transfer functions and signals:

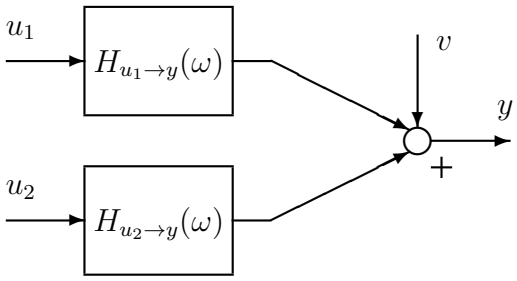

Figure 4. Diagram of a two-input, single-output system.

Signals u_1 and u_2 are inputs to the system, which are represented by transfer function blocks $H_{u_1 \to y}(\omega)$ and $H_{u_2 \to y}(\omega)$. Signal v introduces measurement noise on the output measurement signal y. It is assumed that the noise disturbance is white and uncorrelated with the inputs u_1 and u_2.

Identifying transfer functions $H_{u_1 \to y}(\omega)$ and $H_{u_2 \to y}(\omega)$ is simple if the input signals u_1 and u_2 are uncorrelated. Uncorrelated inputs are obtained in practice by exciting each control surface independently, justifying why frequency sweep experiments are executed for one control surface at a time. To prevent biases due to correlation between the measurement noise and the inputs,[2] it is best to perform open-loop experiments. Operating in open-loop is particularly beneficial for systems equipped with sensors that are susceptible to high levels of measurement noise. Under these conditions, the spectral input-output relationship is given

by the following equation:

$$S_{y,y}(\omega) = |H_{u_1 \to y}(\omega)|^2 \, S_{u_1,u_1}(\omega) + |H_{u_2 \to y}(\omega)|^2 \, S_{u_2,u_2}(\omega) + S_{v,v}(\omega) \tag{21}$$

In this relationship, $S(\omega)$ represents a complex-valued spectral density function. $H_{u_1 \to y}(\omega)$ and $H_{u_2 \to y}(\omega)$ are obtained from cross- and auto-spectral density functions for the input and output signals:

$$H_{u_1 \to y}(\omega) = \frac{S_{y,u_1}(\omega)}{S_{u_1,u_1}(\omega)} \qquad H_{u_2 \to y}(\omega) = \frac{S_{y,u_2}(\omega)}{S_{u_2,u_2}(\omega)} \tag{22}$$

Spectral quantities are estimated from the input and output flight data. For more details on spectral analysis, see References 3 and 23. Applying a standard Hanning window with 50% overlap is one simple approach to obtain a smooth frequency response estimate. Experience has shown that this windowing technique works well for aircraft systems. An appropriate window length remains to be selected. Window length is directly related to the low frequency limit of the estimated frequency response, where longer windows allow lower frequencies. The maximum window length is given by the data record length, which in this case is 10 seconds. Longer windows, however, reduce the total number of windows applied to the data record and diminish the averaging effect. As a result, the estimated frequency response exhibits more random error, particularly at frequencies where the SNR is low and averaging would have been the most helpful. Hence, there is no single optimal window length that provides both high accuracy and broad dynamic range in an estimated frequency response.

A frequency response estimate can be improved by using data from several individual frequency responses, each obtained with a different window length, to form a composite frequency response. The composite frequency response blends the averaging benefits of shorter windows with the dynamic range advantages of longer windows. In this analysis, 5 frequency responses are obtained using 2, 4, 6, 8, and 10 second windows. The basic principle used to generate the composite frequency response emphasizes frequency response data from the response with the highest coherence at each individual frequency point. Coherence functions, denoted $\gamma^2(\omega)$, measure the linear correlation between signals. For example, a coherence value of 1 indicates that the entire output response is accounted for by the input via a linear transfer function. Hence, the composite frequency response is generated by emphasizing data from the frequency response with the highest coherence. More complex optimization-based approaches have been developed to obtain more accurate composite frequency responses.[3] However, coherence weighting alone yields sufficiently accurate results for small UAVs.

In general, coherence values less than one imply the presence of "non-ideal" effects in the input-output relationship, such as nonlinear dynamics, unmeasured inputs, disturbances, or

measurement noise. High coherence, in practice above 0.7, is desired for accurate frequency domain system identification. Coherence functions for the system in Figure 4 based on spectral density functions, assuming uncorrelated inputs, are given by:

$$\gamma^2_{u_1,y}(\omega) = \frac{|S_{y,u_1}(\omega)|^2}{S_{u_1,u_1}(\omega)\ S_{y,y}(\omega)} \qquad \gamma^2_{u_2,y}(\omega) = \frac{|S_{y,u_2}(\omega)|^2}{S_{u_2,u_2}(\omega)\ S_{y,y}(\omega)} \tag{23}$$

Transfer functions $H_{u_1\to y}(\omega)$ and $H_{u_2\to y}(\omega)$ are used as estimates for the system frequency response in the subsequent parametric identification analysis. This basic insight on the spectral estimation process must be incorporated into the design of flight experiments in order to achieve the most accurate frequency response estimates.

B. Parametric Identification

The longitudinal and lateral/directional aircraft dynamics are identified by fitting their corresponding linear parametric models to estimated frequency responses. This is implemented as a nonlinear optimization that aims to minimize the error of the fit in the frequency domain. The decision variables in the optimization are the stability and control derivatives from the state and input matrices of the linear parametric models. Hence, the identification subspace is described by the set of aerodynamic parameters that determine the state-space representation of the aircraft dynamics. The optimization uses a cost function to capture errors in the frequency domain (over a desired interval) between the linear parametric models and the estimated frequency responses. The cost function is weighted based on high coherence to emphasize the fit where the estimated frequency responses accurately capture the system response.

The ability to identify a physically meaningful aircraft model depends on the number of free parameters in the linear model relative to the information captured by the estimated frequency responses. In general, the information captured is limited by the available sensor measurements and the experimental constraints. Small, low-cost UAVs are equipped with a limited quantity of sensors, which restricts the number of available estimated frequency responses. Furthermore, the 10 second experiment time window for the Ultra Stick 25e implies that the phugoid mode cannot be excited. This mode is also significantly decoupled from the remaining longitudinal dynamics. Including free parameters in the optimization that describe this non-excited, decoupled mode would result in over-parametrization. To address this issue, parameters associated with the phugoid mode are fixed to their baseline values. This assumption can introduce errors in the identified model in the form of a low frequency mismatch. However, low frequency errors can easily be handled by feedback control and hence are not of great concern.

Flight dynamics relevant for control applications can be identified with the proposed ap-

proach using measurements from an IMU alone. This is a significant advantage for low-cost systems with limited sensor equipment. Other approaches, such as the state-space formulation of the equation-error method,[4] require measurement of every state of the aircraft model. This is not a feasible requirement for low-cost UAVs. Frequency domain parametric identification also has some general advantages over time domain identification. Flight dynamics relevant to control are dominant in a particular frequency range. Identification in the frequency domain allows accurate modeling to be emphasized in this frequency range.

The parametric identification is performed using CIFER®, a frequency domain system identification tool in the aerospace industry.[3] Originally developed for rotorcraft identification, this tool has also been applied to fixed-wing aircraft.[12,14] A nonlinear optimization is implemented for the parametric identification, emphasizing a close model fit in portions of the frequency response with high coherence. Additional known dynamics, such as actuator dynamics and system time delay, can be augmented to the linear parametric models. These additional dynamics allow the optimization to identify a model that closely matches the estimated frequency responses. Actuator dynamics and system time delay are identified separately using a method described in the next section.

VI. Identification Results

The longitudinal and lateral/directional Ultra Stick 25e models are identified separately. The simple structure of the short-period model is exploited first to identify the actuator dynamics and system time delay using the concept of Low-Order Equivalent Systems (LOES). This approach which was originally developed in the 1970s to certify aircraft handling qualities.[24] Parametric identification in CIFER® is performed using the linear aircraft models presented in Section II to determine the longitudinal and lateral/directional flight dynamics.

1. Longitudinal Dynamics

Figure 5 shows the estimated frequency responses and the final parametric identification results for the elevator input to the pitch rate and z-axis acceleration measurements. The frequency response for the pitch rate is on the left, and for the z-axis acceleration on the right. The baseline model is also shown for comparison, indicating a significant deviation from the final results.

The short-period mode has a known structure that can be fitted with a LOES.[12] Analysis based on LOES is performed first in order to identify the actuator dynamics and system time delay. Once these additional dynamics have been determined, they are appended to the short-period state-space model and fixed for the parametric identification in CIFER®. This approach is expected to introduce errors in the final identification results. However, it is

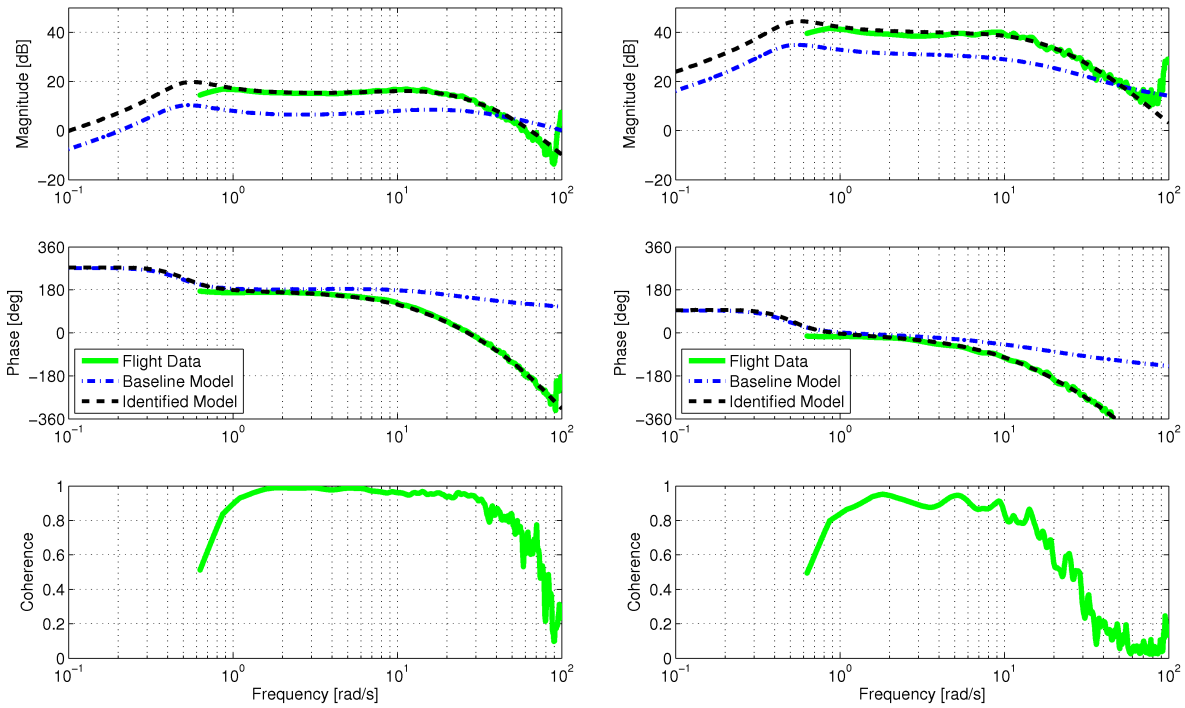

(a) Elevator input to pitch rate.

(b) Elevator input to z-axis acceleration.

Figure 5. Longitudinal dynamics identification for elevator input.

necessary in order to avoid having too many free parameters that need to be identified. LOES modeling is based on using on a transfer function plus a time delay to match an experimental frequency response. The transfer function for the elevator to pitch rate response, which represents the short-period mode, is given by the following:

$$H_{sp}(s) = \frac{K_{sp}(s + a_{sp})}{s^2 + 2\xi_{sp}\,\omega_{sp}s + \omega_{sp}^2} \tag{24}$$

This transfer function has relative degree one, hence its frequency response must exhibit a first order roll-off. The corresponding estimated frequency response on the left in Figure 5, however, exhibits a third order roll-off. This mismatch suggests that the actuator dynamics should be modeled as a transfer function with relative degree two.

Parameters in Equation 24 are tuned to fit the estimated frequency response up to the bandwidth of the short-period mode. The resulting LOES short-period model has a natural frequency ω_{sp} = 17.3 rad/s, damping ratio ξ_{sp} = 0.65, gain K_{sp} = -107.4, and zero a_{sp} = 14.5 rad/s. The actuator is identified as a second-order low-pass filter with a 50.27 rad/s bandwidth. Together, the LOES short-period model and the actuator dynamics provide a good fit of the magnitude curve. A 50 msec first-order Pade approximation is included to model the system time delay, which provides a good fit of the phase curve. Part of this delay is attributed to the 20 msec computer computation time. The remaining time delay captures

unmodeled and higher-order dynamics, such as the nonlinear effect of actuator rate limits.

Parametric identification is used to fit the short-period state-space model (shown in Equation 16) to the estimated frequency responses, given fixed actuator dynamics and system time delay. The results are used to update the baseline model, which completes the longitudinal axis identification process. Derivatives corresponding to the phugoid mode are not updated since they are fixed to their baseline values. The final identified model is shown by the frequency responses in Figure 5. The results indicate that the identified model successfully captures the longitudinal dynamics of the Ultra Stick 25e, along with actuator dynamics and time delay. Based on the coherence functions, the model is expected to be accurate from 1 rad/s up to 70 rad/s in the angular rate channel, and up to 20 rad/s in the acceleration channel. Dynamics near the bandwidth are most important for control applications, and the results indicate that they are captured accurately by the identified model. Table 4 summarizes the modal characteristics of the longitudinal dynamics.

Table 4. Identified longitudinal dynamics of the Ultra Stick 25e.

Mode	Frequency [rad/s]	Damping	Time Constant [s]
Phugoid	0.51	0.38	12.32
Short-Period	16.33	0.83	0.39
Actuator	50.27	0.80	0.13
Time Delay	-	-	0.05

Equation 25 provides the system matrices that represent the identified model shown in Figure 5 and Table 4. Note that the stability and control derivatives corresponding to the phugoid dynamics are maintained at their baseline values.

$$A_{lon} = \begin{bmatrix} -0.38 & 0.60 & -0.36 & -9.80 \\ -0.98 & -10.65 & 16.74 & -0.21 \\ 0.18 & -5.39 & -16.55 & 0 \\ 0 & 0 & 1 & 0 \end{bmatrix} \quad B_{lon} = \begin{bmatrix} -0.36 \\ -3.62^{a} \\ -141.57 \\ 0 \end{bmatrix} \tag{25}$$

The identified model deviates significantly from the baseline model, notable particularly from the magnitude plots in Figure 5. Further, a standard oscillatory short-period mode is identified and shown in Table 4. The poor accuracy of the baseline model is attributed to the approximations made during its construction.

[a] Parametric identification found the cost function to be highly insensitive to the $Z_{\delta_{elev}}$ control derivative, indicating poor accuracy in the identified value of this parameter. The derivative was fixed at the baseline value and the optimization reconverged for the remaining parameters. More details in Section VIII.

2. *Lateral/Directional Dynamics*

The lateral/directional dynamics are more complicated to identify than the longitudinal dynamics. Although the spiral mode is very slow and cannot be excited given the experimental constraints, it cannot be decoupled in the state-space model and fixed to a baseline value. As a result, the lateral/directional model has a large number of free parameters relative to the information captured by the estimated frequency responses. Low gain in some cross-coupling relationships, such as in the rudder to roll rate channel, complicate the problem further.

The lateral/directional actuator model is assumed to be the same as in the longitudinal dynamics. This assumption is valid because all control surfaces are actuated by the same type of servo. The time delay, in general, captures unmodeled and higher-order effects and hence could be different in the lateral/directional axes. However, it is assumed that the time delay is the same throughout the aircraft to avoid introducing another unknown parameter. These assumptions simplify the lateral/directional identification problem, for which over-parametrization is already a significant concern. Figure 6 shows the identification results for the aileron and rudder control surface inputs to the roll rate response. Figure 7 shows the yaw rate response, and Figure 8 shows the y-axis acceleration response.

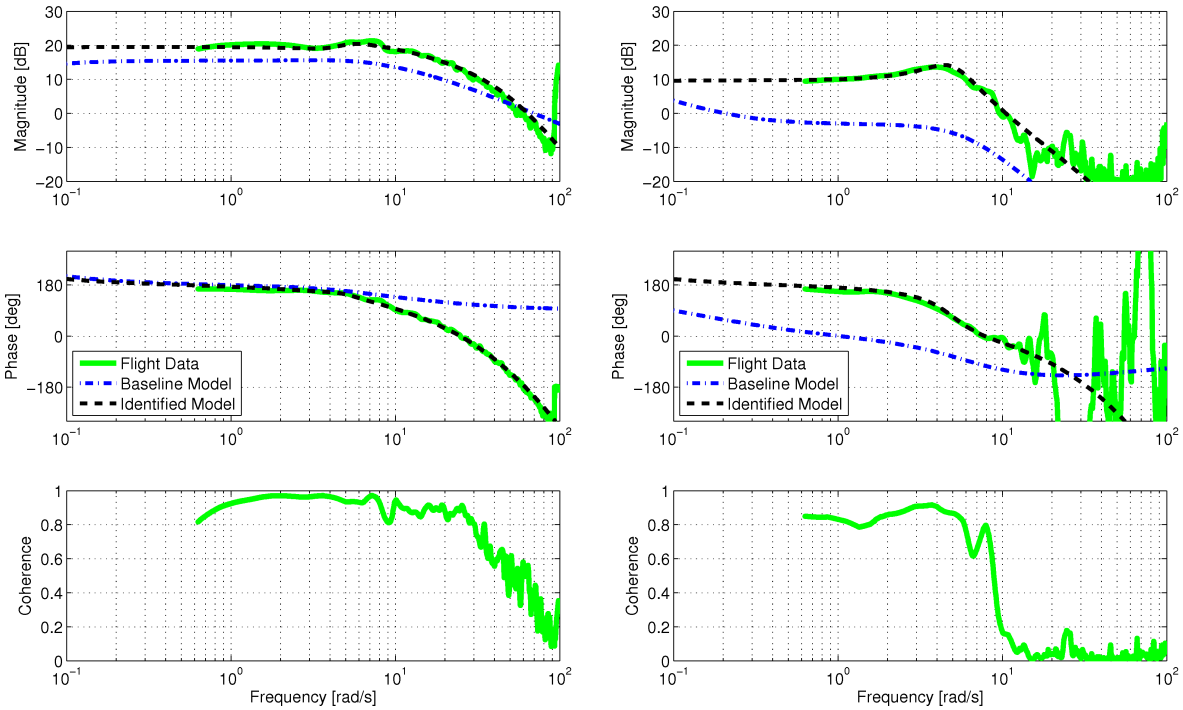

(a) Aileron input to roll rate.

(b) Rudder input to roll rate.

Figure 6. Lateral/directional dynamics identification for roll rate output.

Figure 6 shows the identification results for the control surface inputs to the roll rate response. Based on the coherence functions, the model is expected to be accurate from

around 1 rad/s to 40 rad/s for the aileron channel, and from around 1 rad/s to 8 rad/s for the rudder channel. The roll rate is expected to be identified accurately throughout the bandwidth of the dynamics for both channels. Note that the aileron dynamics roll off at -20 dB/dec, while the rudder dynamics roll off at -40 dB/dec. As a result, gain in the rudder channel is attenuated more at higher frequencies. This is confirmed by the coherence function dropping at a lower frequency in the rudder channel than in the aileron channel.

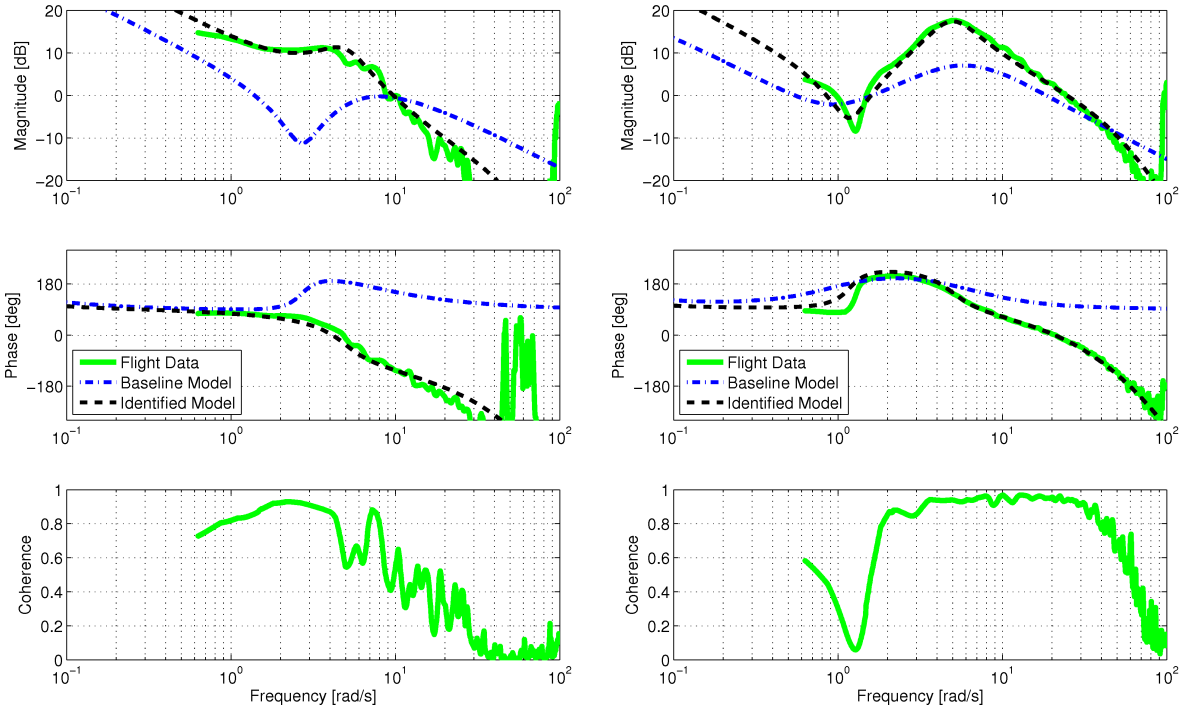

(a) Aileron input to yaw rate.

(b) Rudder input to yaw rate.

Figure 7. Lateral/directional dynamics identification for yaw rate output.

Figure 7 shows the identification results for the control surface inputs to the yaw rate response. Gain in the aileron to yaw rate channel is about 10 dB lower than in the aileron to roll rate channel, which reduces quality in the estimated frequency response due to lower SNR. The aileron to yaw rate channel is accurately modeled from around 1 rad/s to 10 rad/s, which captures the bandwidth of the dynamics. The rudder to yaw rate dynamics show a pair of complex-conjugate zeros near 1 rad/s. The frequency response has low gain near this frequency, which makes the damping of the zero dynamics challenging to identify. This effect is confirmed by the low coherence function in the neighborhood of 1 rad/s in the rudder to yaw rate channel. Overall, the rudder to yaw rate channel is accurately modeled from 2 rad/s to 70 rad/s, which captures the bandwidth of the dynamics.

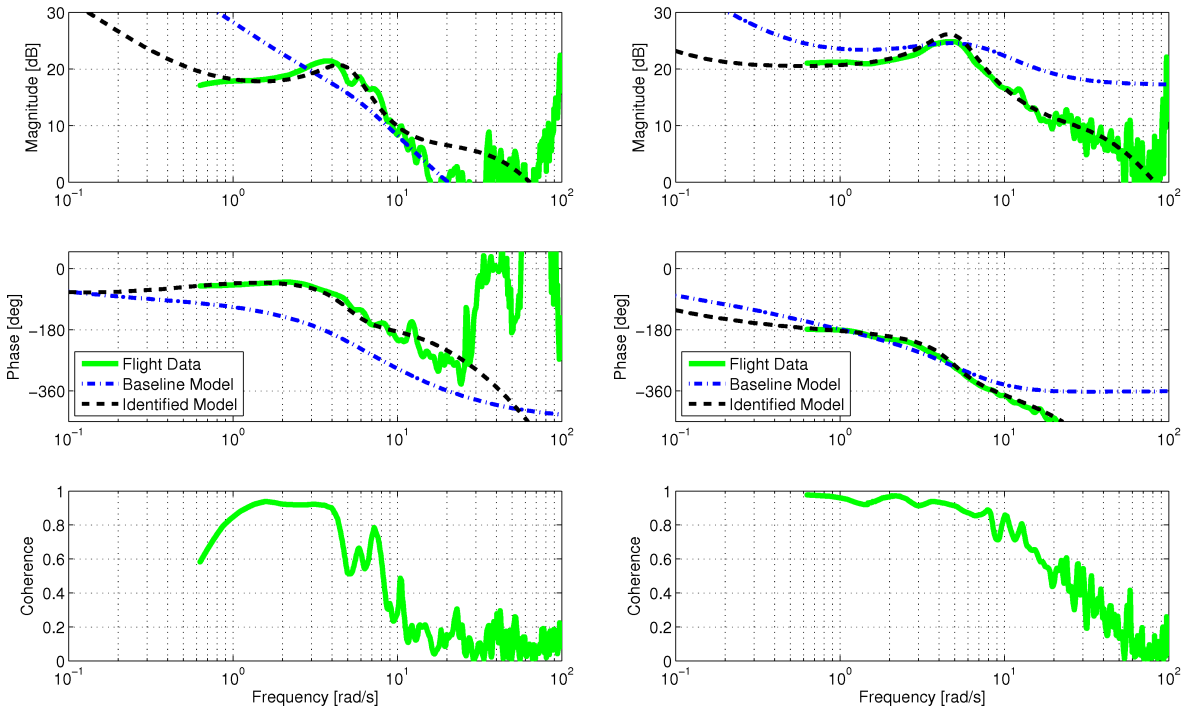

(a) Aileron input to y-axis acceleration.

(b) Rudder input to y-axis acceleration.

Figure 8. Lateral/directional dynamics identification for y-axis acceleration output.

Figure 8 shows the identification results for the control surface inputs to the y-axis acceleration response. The coherence function in the aileron channel is only sufficiently high from 1 rad/s to 4 rad/s, which is a narrower range than desired. The bandwidth of this frequency response is not accurately identified due to a sharp drop in the gain. The rudder to y-component acceleration has higher gain than the aileron. Hence, the coherence function is high and the model is accurately identified from 1 rad/s to 20 rad/s, which covers the relevant dynamic range.

Table 5 summarizes the modal characteristics of the identified lateral/directional dynamics. The slow response associated with the spiral mode is impossible to excite given the prevailing experimental constraints. This is expected to lead to poor identification of the spiral mode. Similar to the phugoid mode, however, this is not a critical issue for control applications. Actuator dynamics and system time delay for the lateral/directional model are assumed to be the same as for the longitudinal model, which were given in Table 4.

Table 5. Identified lateral/directional dynamics of the Ultra Stick 25e.

Mode	Frequency [rad/s]	Damping	Time Constant [s]
Spiral	0.02	-	314.16
Dutch Roll	4.96	0.33	1.27
Roll	12.53	-	0.50

The identified A'_{lat} and B'_{lat} matrices are presented in Equation 26. Unlike for the longitudinal case, the entire set of lateral/directional stability and control derivatives are updated. The matrix M_{lat} is not updated since the mass properties are assumed to be known.

$$A'_{lat} = \begin{bmatrix} -0.64 & 0.46 & -18.21 & 9.50 & 0 \\ -2.02 & -12.47 & 4.05 & 0 & 0 \\ 1.30 & 0.86 & -3.09 & 0 & 0 \\ 0 & 1 & 0.03 & 0 & 0 \\ 0 & 0 & 1 & 0 & 0 \end{bmatrix} \quad B'_{lat} = \begin{bmatrix} -2.06 & 2.98 \\ -139.10 & 6.52 \\ 17.22 & -26.42 \\ 0 & 0 \\ 0 & 0 \end{bmatrix} \tag{26}$$

The results in Figures 6 - 8 indicate that the identified lateral/directional model is most accurate in the roll rate response due to both aileron and rudder inputs, and for the yaw rate and y-component acceleration due to rudder input. Overall, the identified model is significantly more accurate than the baseline model in all channels. This first iteration of frequency domain system identification provides crucial insight regarding the true aircraft dynamics of the Ultra Stick 25e. The findings also provide guidelines for the design of additional flight experiments to be used in refining the model.

VII. Time Domain Model Validation

The accuracy of an identified model is ultimately predicated on its ability to predict responses. For validation purposes, the identified model is simulated using pilot inputs recorded from a doublet flight maneuver. Simulation results are compared to flight data using the Theil Inequality Coefficient (TIC).[25] The TIC is a normalized metric between 0 and 1 used to compare time histories, where 0 indicates a perfect match and 1 indicates a worst case deviation. Values of TIC < 0.25 correspond to accurate predictions for fixed-wing aircraft.[3,26] The TIC is defined by the following relationship:

$$\text{TIC} = \frac{\sqrt{\frac{1}{n}\sum_{i=1}^{n}(x_i - \tilde{x}_i)^2}}{\sqrt{\frac{1}{n}\sum_{i=1}^{n}x_i^2} + \sqrt{\frac{1}{n}\sum_{i=1}^{n}\tilde{x}_i^2}}, \tag{27}$$

where x is the simulation time history, $\tilde{x}$ is the flight data time history, and n is the number of data samples. Although the identified model is linear, the aerodynamic derivatives can be extracted and integrated into in the nonlinear equations of motion. The resulting nonlinear model is also simulated using the doublet input signal, and the TIC is computed.

The doublet input signal is comprised of an elevator doublet, followed by an aileron doublet, and completed with a rudder doublet. The results are shown in Figure 9. Pilot

command signals are plotted on the same axis as their corresponding primary angular rates. The corrections made with the aileron and elevator at the end of the maneuver are used to return the aircraft to its original trim condition.

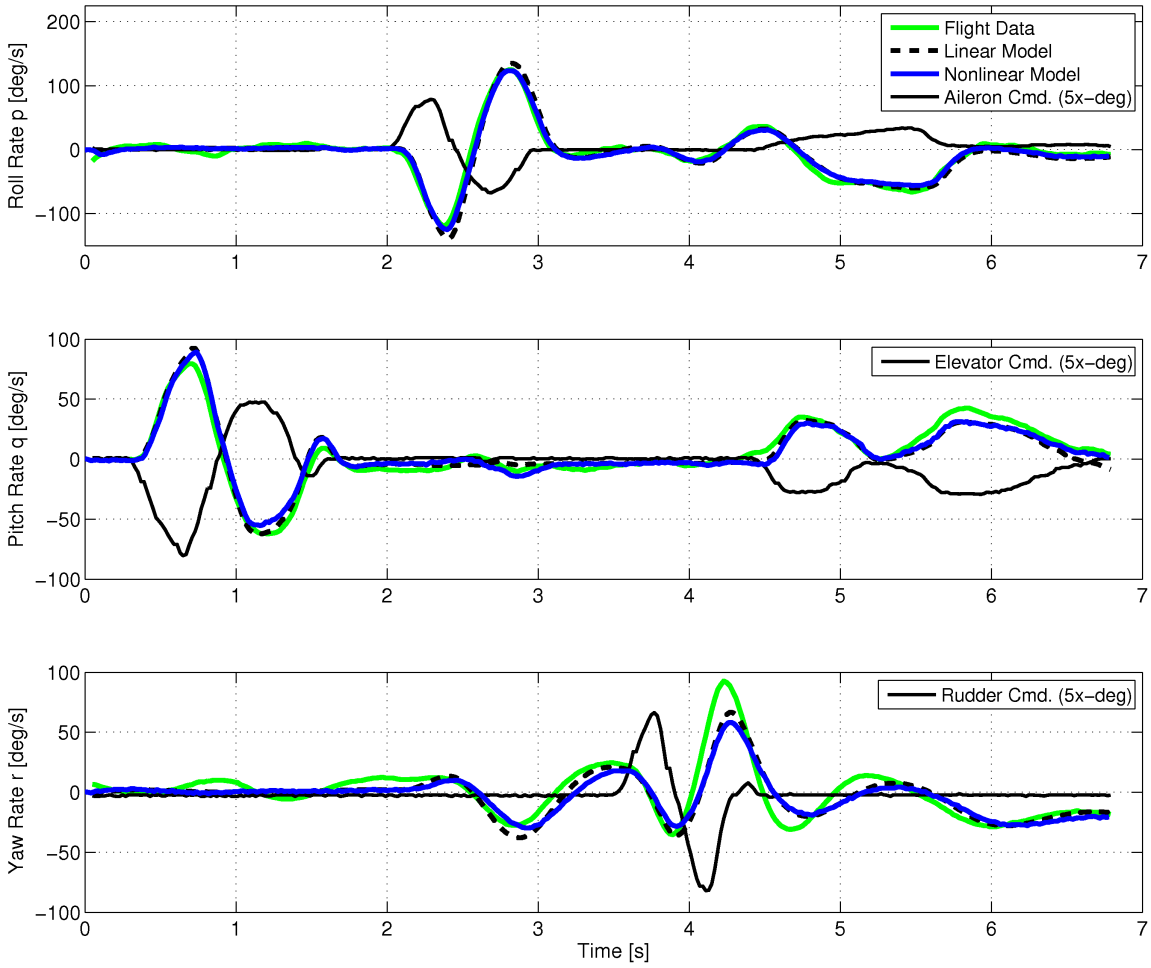

Figure 9. Time domain model validation of the identified Ultra Stick 25e dynamics.

Figure 9 shows that the identified models accurately predict the aircraft response, and moreover, that the linear and nonlinear responses match closely. The elevator doublet response confirms that the longitudinal and lateral/directional dynamics are mostly decoupled. Roll and pitch rate responses are captured with high accuracy, and their nonlinear models yield TIC values of 0.07 and 0.12, respectively. The yaw rate response exhibits a slight discrepancy from the identified models, yielding a TIC value of 0.26 for the nonlinear case. This is near the limit for accurate models. The mismatch is attributed to low damping in the dutch roll mode that was not captured with sufficient accuracy by the flight experiment. Coupling between the pitch and yaw axes (seen in the flight data) can be attributed to unmodeled asymmetries in the airframe and the neglected motor effects.

VIII. Sensitivity and Residual Analysis

The process of validating model accuracy is extended beyond time domain validation with a sensitivity and residual analysis. Analysis presented in Reference 3 is used to construct an uncertainty model based on sensitivities to parameter variation. Residuals obtained from the spectral analysis are used to generate an output disturbance model. Together, the uncertainty and disturbance models complement the identified model and provide additional insight into its accuracy.

A. Sensitivity to Parameter Variation

Uncertainty in the identified model is quantified using properties of the converged cost function from the parametric identification process. This cost function depends on the identified parameters and captures the model fit error in the frequency domain. Its sensitivity to parameter variations, or combinations of parameter variations, is used to model uncertainty. Cramér-Rao (CR) bounds represent this type of sensitivity in the cost function, and hence are used as a basis for a parametric uncertainty model.

CR bounds depend on the diagonal entries of the inverse Hessian matrix $\mathcal{H}^{-1}$, evaluated for the converged cost function. The Hessian matrix is estimated and CR bounds are calculated as part of the identification process. A large CR_i bound indicates either low curvature in the cost function (high insensitivity) with respect to the ith parameter, or that the ith parameter is correlated with another parameter.[3] Separately, CR bounds also represent a lower bound on the standard deviation σ of the statistical scatter expected from running multiple experiments.[2,3] This is shown by the following relationship:

$$\sigma_i \geq CR_i = \sqrt{(\mathcal{H}^{-1})_{ii}} \tag{28}$$

Experience has shown that a factor of 2 can be used to obtain an approximation of the standard deviation, resulting in Equation 29:[3]

$$\sigma_i \approx 2CR_i = 2\sqrt{(\mathcal{H}^{-1})_{ii}} \tag{29}$$

A parametric uncertainty model is constructed based on CR bounds. The uncertainty describes a family of identified models expected from running multiple experiments. High CR bounds are attributed to several factors. For example, a parameter may be physically insignificant with respect to the measured aircraft response. This kind of parameter is difficult to identify and hence associated with a high CR bound. Reduced coherence in the estimated frequency response can also lead to high CR bounds. Due to weighting based on high coherence in the identification process, low coherence can mask the effect of varying a

parameter. Finally, correlation between parameters indicates that they can vary together, making their individual values difficult to determine. Relating parametric uncertainty to CR bounds is one way to collect these identification problems and form a comprehensive uncertain aircraft model.

The uncertainty model is constructed by letting the model parameters vary on an interval centered at their nominal identified values. Each parameter is modeled as a fixed interval uniform distribution. This type of model is useful since it can be analyzed directly with existing robustness tools, such as μ-analysis. To provide a conservative estimate of the uncertainty, the interval is selected to include 3 standard deviations from the nominal value.[8] Figure 10 illustrates how uncertainty in all the parameters manifests as a variation in the frequency response. The uncertainty model is randomly sampled to generate a family of frequency responses. In this example, two families of frequency responses are shown. The aileron input to roll rate channel is on the left, and the rudder input to yaw rate channel is on the right. The nominal identified model is highlighted by the darker dashed curves.

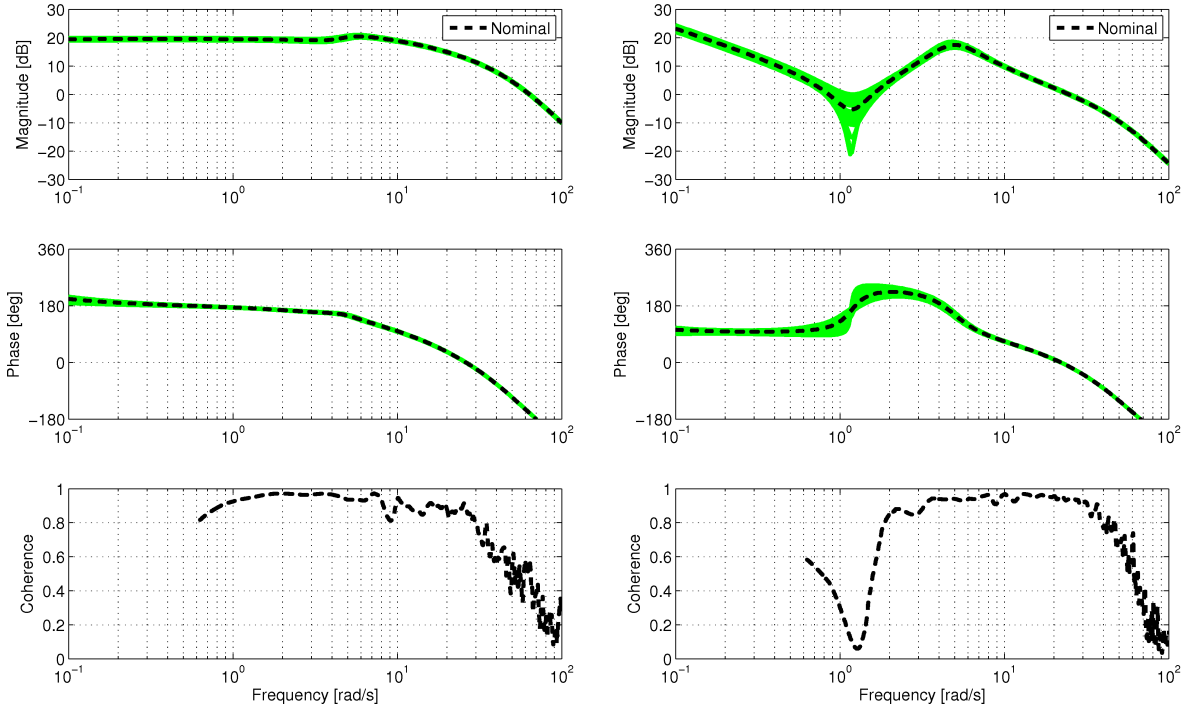

(a) Aileron input to roll rate.

(b) Rudder input to yaw rate.

Figure 10. Selected uncertain frequency responses.

Figure 10 is useful because it provides a visual representation of the expected variation in the frequency response due to parametric uncertainty. The aileron to roll rate channel is accurately identified, as indicated by the high coherence function. Accordingly, low variation due to uncertainty is noted. The rudder to yaw rate model, however, is poorly identified near 1 rad/s. This is due to low gain in the transfer function. Uncertainty is high due to the

low coherence, and significant variation is noted in the frequency response. The uncertainty shows that the damping of a pair of complex conjugate zeros in the transfer function is not accurately modeled. Due to the low coherence, the optimization is unable to determine the damping, which leads to high uncertainty in the identified parameters of that mode.

The effect of uncertainty must be considered in every relevant input-output channel. Exhaustive analysis of each remaining channel in the aircraft model is left out in the interest of brevity. However, visualizing the uncertainty is a straightforward process. The full set of CR bounds obtained from the identification process (including the factor of 2) is given in Table 6. The bounds are given as percentage deviations from the nominal identified values of their corresponding aerodynamic derivatives, which were provided in the identified system matrices.

Table 6. Cramér-Rao bounds for the identified aircraft model.

Deriv.	$2CR$ (%)	Deriv.	$2CR$ (%)	Deriv.	$2CR$ (%)	Deriv.	$2CR$ (%)
Z_w	14.88	Y_v	5.17	L_v	9.16	N_v	3.49
Z_q	8.41	Y_p	20.20	L_p	8.20	N_p	16.30
$Z_{\delta_{elev}}$	(129.4)	Y_r	0.74	L_r	16.82	N_r	6.58
M_w	20.69	$Y_{\delta_{ail}}$	38.42	$L_{\delta_{ail}}$	7.25	$N_{\delta_{ail}}$	7.07
M_q	16.28	$Y_{\delta_{rud}}$	11.96	$L_{\delta_{rud}}$	41.94	$N_{\delta_{rud}}$	4.34
$M_{\delta_{elev}}$	8.49						

The CR bounds indicate that most parameters are identified accurately. Experience has shown that identification results are reliable when most $2CR_i < 20\%$.[3] The rule of thumb is exceeded significantly by the $Z_{\delta_{elev}}$ parameter. This derivative represents the elevator z-axis force, which has a limited effect on the response relative to other forces and moments acting on the aircraft. The manifestation of the elevator z-axis force on a_z and q is negligible, and hence $Z_{\delta_{elev}}$ can vary greatly without having a significant impact on the measured input-output dynamics (or the cost function). Due to insensitivity in the cost function,[3] noted by the 129.4% CR bound, the identified value is nearly arbitrary. Therefore, $Z_{\delta_{elev}}$ was fixed at the baseline value and the optimization reconverged for the remaining parameters. The original CR bound associated with $Z_{\delta_{elev}}$, however, was retained as uncertainty.

The $Y_{\delta_{ail}}$ and $L_{\delta_{rud}}$ derivatives represent cross-coupling relationships with low gain for the Ultra Stick 25e, which elevates their CR bounds. $Y_{\delta_{ail}}$ represents the aileron effectiveness in generating a y-axis force. $L_{\delta_{rud}}$ represents the rudder effectiveness in generating a rolling moment. It is difficult to obtain measurements with sufficiently high SNR and estimate accurate frequency responses for these relationships, primarily due to their low gain. As a result, errors and variations in the model fit are not significantly penalized in the parametric identification process, which results in elevated CR bounds for $Y_{\delta_{ail}}$ and $L_{\delta_{rud}}$.

B. Residual Disturbance Modeling

The effect of disturbances acting on the aircraft is captured by residual spectra computed for the output measurements. Residual spectra contain the portion of the output measurement that cannot be accounted for by the inputs via linear transfer functions. For this analysis, residual spectra are computed for the three angular rate measurements. An output disturbance model is generated, which complements the identified aircraft model.

The system diagram in Figure 4 shows the identification problem cast for a two-input, single output system. In the ideal scenario, the system is linear and subject to a white noise output disturbance v. Hence, the output disturbance is uncorrelated with the inputs. The inputs and outputs are related via linear transfer functions, and the coherence functions have values near 1. Therefore, in ideal conditions, the residual spectrum for the output is white noise. The output residual spectrum is computed with the following relationship:[23]

$$S_{v,v}(\omega) = [1 - \gamma^2_{u,y}(\omega)]S_{y,y}(\omega) \tag{30}$$

In practice, these ideal conditions cannot be fully satisfied because the aircraft is not a linear system and the output disturbance is not white noise. The effects of nonlinear dynamics, wind gusts, turbulence, and correlated noise on the measured output are compounded into the output residual spectrum. Hence, the inputs and outputs are no longer perfectly related via linear transfer functions, as assumed by the ideal scenario and in conjunction with Equation 30.

The residual spectrum of the output (computed with Equation 30) is used to infer a disturbance model for the aircraft dynamics. The disturbance on the measured output is modeled with a transfer function, denoted $D_y(\omega)$. This transfer function is driven by a unit amplitude white noise input signal v. The magnitude of the disturbance model transfer function is given by the following equation:

$$|D_y(\omega)| = \sqrt{|S_{v,v}(\omega)|} \tag{31}$$

Disturbance models are computed for the three angular rate measurements on the Ultra Stick 25e. Spectra and coherence functions obtained from the frequency sweep experimental data are used in this analysis. Figure 11 shows a diagram that describes how the output disturbance enters the system. Three estimated transfer functions (obtained using Equation 22) relate the inputs to their primary angular rate responses. In the longitudinal axis, the disturbance model $D_q(\omega)$ is calculated for the elevator to pitch rate channel. In the lateral/directional axes, disturbance model $D_p(\omega)$ is calculated for the aileron to roll rate channel, and disturbance model $D_r(\omega)$ is calculated for the rudder to yaw rate channel.

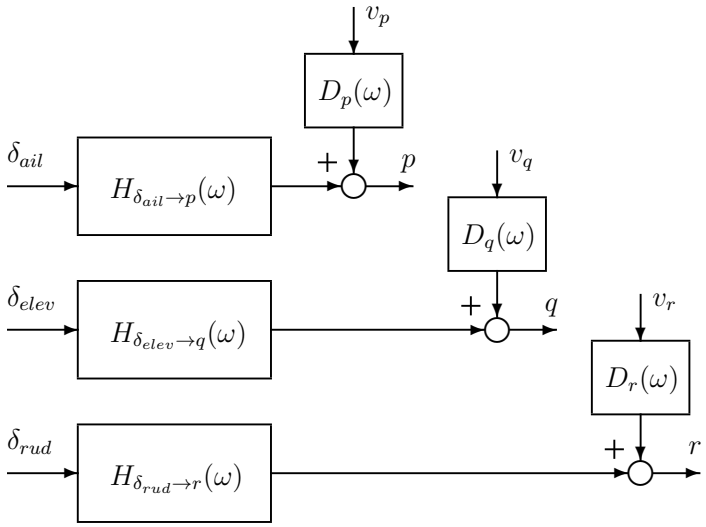

Figure 11. System diagram for output disturbance modeling.

The computed disturbance models are presented in Figure 12. Coherence functions are included below as a reference to indicate the predicted accuracy of the identified model. The roll rate disturbance model $D_p(\omega)$ is shown on the left, the pitch rate disturbance model $D_q(\omega)$ in the middle, and yaw rate disturbance model $D_r(\omega)$ on the right. The results show that the output disturbance entering the system is not white noise, as assumed in the ideal scenario. This discrepancy can be attributed to the effects of nonlinear dynamics, wind gusts, turbulence, and correlated noise on the measured output.

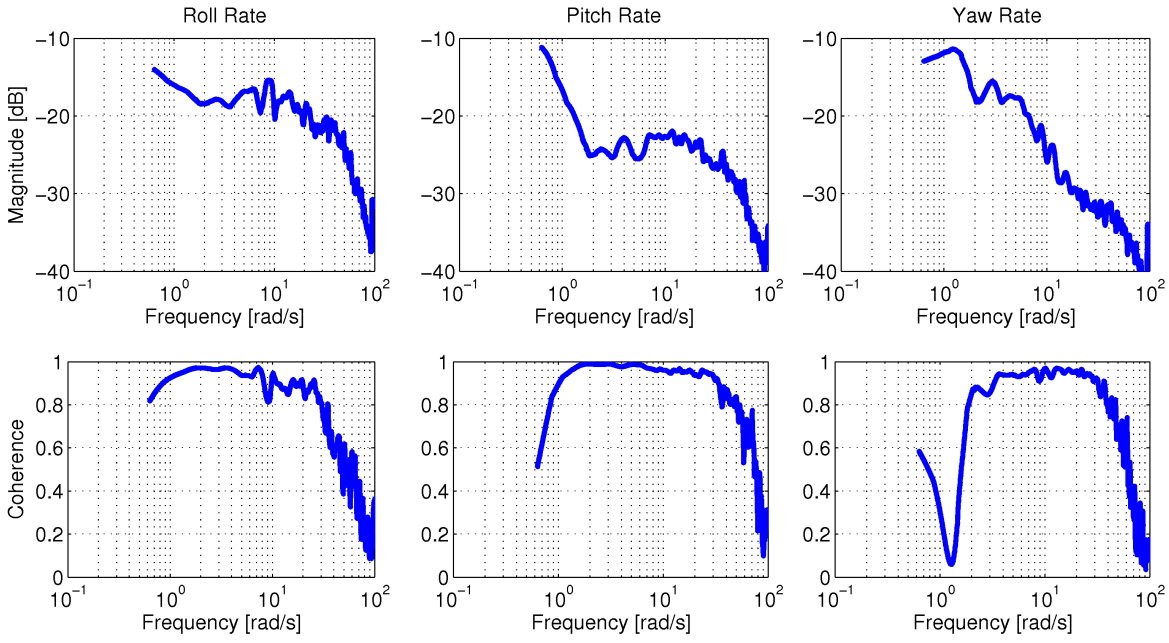

Figure 12. Output disturbance models for angular rate measurements.

The expected output disturbance is the measurement noise introduced by the IMU sensor. For each angular rate channel, noise with amplitude $\pm$ 2 deg/s is observed. This type of noise corresponds to a disturbance model with flat magnitude near -29 dB. However, the magnitudes of all three disturbance models in Figure 12 are greater than -29 dB, indicating the presence of additional disturbances. Moreover, the disturbance models are qualitatively similar in frequency domain characteristics to their corresponding identified aircraft models. For example, the roll rate disturbance model on the left in Figure 12 is similar to the aileron to roll rate identified model on the left in Figure 6. The two models have similar bandwidth and roll-off characteristics. The same finding holds for the pitch and yaw rate disturbance models. This general observation suggests that input disturbances dominate the total disturbances captured in the measured aircraft response.

Input disturbances propagate through the aircraft dynamics, and their effects manifest directly on the residual output spectra (such as those shown in Figure 12). Hence, each output residual spectrum is "colored" with the aircraft dynamics, which means they have similar frequency domain characteristics. The results in Figure 12 indicate that the disturbance models are "colored" with the identified aircraft dynamics. Therefore, disturbances acting on the input, such as wind gusts or turbulence, dominate the disturbances acting directly on the output, such as sensor noise. This result is important for understanding key performance limitations of small, low-cost UAVs. In particular, it shows that although low-cost sensors, such as the IMU on the Ultra Stick 25e, are susceptible to high levels of noise, the presence of noise is not significant in comparison to the effect of wind gusts or turbulence experienced by the aircraft.

IX. Conclusion

A practical system identification procedure was developed to accurately model the dynamics of small, low-cost, fixed-wing UAVs. The procedure addresses requirements and good practices to obtain models that are useful in control applications for aircraft equipped with a limited set of low-cost sensors. The approach to system identification is based on estimating frequency responses, which are obtained using flight data. Aircraft dynamics are identified in the frequency domain by fitting linear parametric models to the estimated frequency responses. The identified models are validated with flight data in the time domain, as well as through a sensitivity and residual analysis. The main advantage of the proposed approach is the successful identification of aircraft dynamics using flight data from a single, low-cost inertial sensor. A drawback to the approach is the multi-step analysis process that cannot be performed in real-time.

Acknowledgments

This research was initiated as a final project for a graduate level course on system identification in the Aerospace Engineering & Mechanics department at the University of Minnesota. The authors would like to specifically thank Ahmet Arda Ozdemir, Paul Freeman, Michael Mott, and Navid Dadkhah for their contribution to this work. The research was also partially supported under the NASA Langley NRA contract NNH077ZEA001N entitled "Analytical Validation Tools for Safety Critical Systems," NASA Langley NNX08AC65A contract entitled 'Fault Diagnosis, Prognosis and Reliable Flight Envelope Assessment" and the US National Science Foundation under Grant No. NSF-CNS-0931931. Any opinions, findings, and conclusions or recommendations expressed in this material are those of the author(s) and do not necessarily reflect the views of NASA or the National Science Foundation.

References

[1]Ljung, L., *System Identification: Theory for the User*, Prentice Hall, 2nd ed., 1999.

[2]Soderstrom, T. and Stoica, P., *System Identification*, Prentice Hall, 2001.

[3]Tischler, M. and Remple, R., *Aircraft and Rotorcraft System Identification*, AIAA, 2006.

[4]Klein, V. and Morelli, E., *Aircraft System Identification: Theory and Practice*, AIAA, 2006.

[5]Jategaonkar, R., *Flight Vehicle System Identification*, AIAA, 2006.

[6]Mettler, B., Tischler, M., and Kanade, T., "System Identification of a Small-Scale Unmanned Rotorcraft for Flight Control Design," *Journal of the American Helicopter Society*, Vol. 47, No. 1, 2002.

[7]Theodore, C., Tischler, M., and Colbourne, J., "Rapid Frequency-Domain Modeling Methods for Unmanned Aerial Vehicle Flight Control Applications," *Journal of Aircraft*, Vol. 41, No. 4, 2004.

[8]Dadkhah, N. and Mettler, B., "System Identification Modelling and Flight Characteristics Analysis of Miniature Co-Axial Helicopter," *Accepted for Publication in Journal of the American Helicopter Society*, 2011.

[9]Gremillion, G. and Humbert, J. S., "System Identification of a Quadrotor Micro Air Vehicle," *AIAA Atmospheric Flight Mechanics Conference and Exhibit*, Toronto, Canada, 2010.

[10]Bachelder, E., Thompson, P., Klyde, D., and Alvarez, D., "A New System Identification Method Using Short Duration Flight Test Inputs," *AIAA Atmospheric Flight Mechanics Conference*, Portland, OR, 2011.

[11]Morelli, E. and Smith, M., "Real-Time Dynamic Modeling: Data Information Requirements and Flight-Test Results," *Journal of Aircraft*, Vol. 46, No. 6, 2009.

[12]Morelli, E., "Low-Order Equivalent System Identification for the Tu-144LL Supersonic Transport Aircraft," *Journal of Guidance, Control, and Dynamics*, Vol. 26, No. 2, 2003.

[13]Murch, A., Dorobantu, A., and Balas, G., "University of Minnesota UAV Flight Control Research Group," http://www.uav.aem.umn.edu.

[14]Dorobantu, A., Murch, A., Mettler, B., and Balas, G., "Frequency Domain System Identification for a Small, Low-Cost, Fixed-Wing UAV," *AIAA Atmospheric Flight Mechanics Conference and Exhibit*, Portland, Oregon, 2011.

[15]Cook, M., *Flight Dynamics Principles*, Elsevier Ltd., 2nd ed., 2007.

[16]"ADIS16405 Triaxial Inertial Sensor with Magnetometer Datasheet," Tech. rep., Analog Devices.

[17]Murch, A., Paw, Y. C., Pandita, R., Li, Z., and Balas, G., "A Low Cost Small UAV Flight Research Facility," *CEAS Conference on Guidance, Navigation, and Control*, Munich, Germany, 2011.

[18]"phyCore MPC5200B-tiny Microcontroller Datasheet," Tech. rep., Phytec.

[19]Hoak, D. E. et al., "The USAF Stability and Control Datcom," Tech. Rep. AFWAL-TR-83-3048.

[20]Owens, B., Cox, D., and Morelli, E., "Development of a Low-Cost Sub-Scale Aircraft for Flight Research: The FASER Project," *25th AIAA Aerodynamic Measurement Technology and Ground Testing Conference*, San Francisco, CA, United States, 2006.

[21]Morelli, E. and DeLoach, R., "Wind Tunnel Database Development Using Modern Experiment Design and Multivariate Orthogonal Functions," *41st Aerospace Sciences Meeting and Exhibit*, Reno, NV, 2003.

[22]MATLAB, *Version 7.14.0.739 (R2012a)*, The MathWorks Inc., Natick, Massachusetts, 2012.

[23]Bendat, J. and Piersol, A., *Engineering Applications of Correlation and Spectral Analysis*, John Wiley & Sons, 1993.

[24]Hodgkinson, J., "History of Low-Order Equivalent Systems for Aircraft Flying Qualities," *Journal of Guidance, Control, and Dynamics*, Vol. 28, No. 4, 2005.

[25]Theil, H., *Economic Forecasts and Policy*, North-Holland Publishing Company, 1970.

[26]Jategoankar, R., Fishenberg, D., and Gruenhagen, W., "Aerodynamic Modeling and System Identification from Flight Data - Recent Applications at DLR," *Journal of Aircraft*, Vol. 41, No. 4, 2004, pp. 681–691.